



RIGOROUS MODELLING OF SOIL-STRUCTURE INTERACTION FOR SEISMIC STRUCTURAL RESPONSES

Hossein RAHNEMA¹ and Behtash JAVIDSHARIFI²

ABSTRACT

Effects of soil-structure interaction (SSI) have proven to be of more importance than to be ignored. On the contrary to the substructuring method which usually assumes linear elastic behaviour for the soil-structure system, direct modelling which is applied in this study may predict nonlinear responses of the structure and its being placed on an inelastic environment. The soil-structure system is modelled and analysed once directly with the UCSD soil model and then compared with substructuring method with the UCD model, both analysed in time domain. The soil is supposed to be comprised of sand with different mechanical properties. Loma Prieta earthquake record (1989) is used to carry out time domain analyses and capture structural responses. The force outputs reveal a decrease when elastoplastic SSI is considered; while displacement amplitudes are found to be more for cases not involving SSI, or involving elastic SSI. The changing of the applied constitutive model as well as mechanical properties of the sand from loose to stiff manifests changes in responses. As the soil gets denser, the SSI behaviour gets closer to the elastic case.

INTRODUCTION

Basic SSI equation

In substructuring methods and whenever else this method is applied in a part of the research, since usually the at-hand recorded motions are those of the free-field, the ground motion, i.e. motion incorporating the excavation and its changes in the dynamic stiffness of the system, is calculated using Eq.(1).

$$\{u_b^g(\omega)\} = [S_{bb}^g(\omega)]^{-1} [S_{bb}^f(\omega)] \{u_b^f(\omega)\} \quad (1)$$

Fig.1 depicts the usage of the above equation in substructuring method of SSI (Mohasseb and Wolf, 1989).

¹ Assistant professor, Shiraz University of Technology, Shiraz, rahnema@sutech.ac.ir

² Construction projects supervisor, Fars Regional Electricity Company, Shiraz, b.javidsharifi@sutech.ac.ir

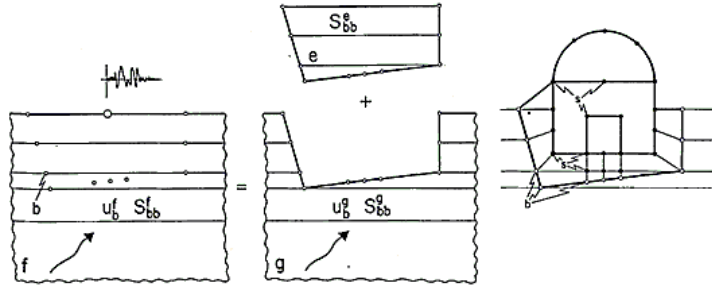


Figure 1. Decomposition of free-field into ground and excavation (after Mohasseb & Wolf, (1989))

The Scaled-Boundary Finite Element Method

The semi-analytical Scaled Boundary Finite Element Method (SBFEM) which is a combination of Finite Element and Boundary Element methods has been implemented to calculate the unit impulse response of the far-field. Program SIMILAR developed by Wolf and Song (1996) has been made use of to carry out SBFEM procedures. The system is decomposed into three regions, namely the structure, the near-field soil and the far-field soil as shown in Fig.2 (Hassanen and El-Hamalawi, 2007).

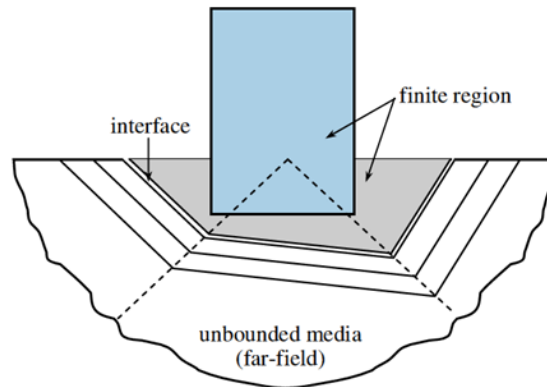


Figure 2. Decomposition of the soil-structure system into three sub-regions (after M.C. Genes, (2012))

Truncating the far-field out of the soil-structure system results in its replacement by forces produced on the hypothetical interface nodes which shake the near-field soil-structure system (Wolf, 2003). Similar solution techniques have been exerted to solve SSI problems. Mustafa Kutaniş and Muzzafer Elmas inspected this issue in 2000 making use of the same procedure (KUTANIŞ and ELMAS, 2009) while framed structures had already been examined in elasto-plastic SSI by J. Noorzai et al. seven years before that (Noorzai et al., 1995). In 2002, M.C. Genes and S. Kocak published their pioneering work on SSI using coupled FEM and SBFEM (Genes and Kocak, 2002) and then generalized their work to layered media in 2005 (Genes and Kocak, 2005). Dynamic Large-scale SSI systems with SBFEM in layered media were inspected in a parallelized coupled procedure by M.C. Genes in 2012 (Genes, 2012). For all carried out works, the soil-structure system has been in need of an input motion. In the book by S.L. Kramer, methods of linear and nonlinear magnification and deconvolution of seismic motions to the depth and surface of a soil column are presented in details covering the works done so far (Kramer, 1996). Based on what is presented there, the time domain input motion is converted to frequency domain using a Fourier transform, and then a frequency domain magnification factor called transfer function is calculated based on the soil material, thickness and damping. Then, using this multiplier, the time domain motion is calculated and interaction forces are determined by convolution integrals convolving unit impulse responses in discretized time and effective input motions (Wolf and Song, 1996).

The unit impulse response matrix is convolved with the accelerogram to yield the interaction forces, as shown in Eq.(2):

$$\{R(t)\} = \int_0^t \left[M^\infty(t-\tau) \left\{ \ddot{u}(\tau) \right\} \right] d\tau \quad (2)$$

where M^∞ is the unit impulse response which is achieved by transforming the dynamic stiffness from frequency domain to time domain (Wolf, 2003). The dynamic stiffness matrix is defined as in Eq.(3) and Eq.(4) for bounded and unbounded media respectively (Wolf, 1985, Wolf, 2003).

$$S(\omega_j) = K - \omega_j^2 m + i \omega_j C \quad (3)$$

$$S^\infty(\omega) \approx i \omega C_\infty + K_\infty + \frac{1}{i \omega} A_l \quad (4)$$

Leaving Eq.(5) for the unit impulse at each individual time step, i.e. dynamic stiffness in time domain:

$$u_j(t) = u(\omega_j) e^{i \omega_j t} \quad (5)$$

where S and S^∞ are dynamic stiffness matrices of the bounded and unbounded domains respectively, (either free-field or ground), C_∞ and K_∞ are respectively radiation damping and static stiffness of the unbounded domain and A_l is a constant. To perform the transformation from frequency domain to time domain and vice versa, Fourier and inverse Fourier Transformations are used (Eq.(6) and Eq.(7)).

$$P(\omega) = \int_{-\infty}^{+\infty} P(t) e^{-i \omega t} dt \quad (6)$$

$$P(t) = \frac{1}{2\pi} \int_{-\infty}^{+\infty} P(\omega) e^{-i \omega t} d\omega \quad (7)$$

After determining the interaction forces which are to be divided between interface nodes, they are inserted in total equations of motion in interaction sense as in Eq.(8):

$$\begin{bmatrix} M_{ss} & M_{sb} \\ M_{bs} & M_{bb} \end{bmatrix} \begin{Bmatrix} \ddot{u}_s^t(t) \\ \ddot{u}_b^t(t) \end{Bmatrix} + \begin{bmatrix} K_{ss} & K_{sb} \\ K_{bs} & K_{bb} \end{bmatrix} \begin{Bmatrix} u_s^t(t) \\ u_b^t(t) \end{Bmatrix} = \begin{Bmatrix} \{0\} \\ -\{R(t)\} \end{Bmatrix} \quad (8)$$

where M_{ss} are the domain mass matrices and K_{ss} are static stiffness matrices. Adding damping to the environment and thus to the formulation, along with embedding the SBFEM formulation inside the total equation of motion will result in Eq.(9):

$$\begin{aligned} & \begin{bmatrix} M_{ss} & M_{sb} \\ M_{bs} & M_{bb} \end{bmatrix} \begin{Bmatrix} \ddot{u}_s^t(t) \\ \ddot{u}_b^t(t) \end{Bmatrix} + \begin{bmatrix} [0] & [0] \\ [0] & [C_\infty] \end{bmatrix} \begin{Bmatrix} \dot{u}_s^t(t) \\ \dot{u}_b^t(t) \end{Bmatrix} + \begin{bmatrix} K_{ss} & K_{sb} \\ K_{bs} & K_{bb} \end{bmatrix} \begin{Bmatrix} u_s^t(t) \\ u_b^t(t) \end{Bmatrix} + \left\{ \int_0^t [S_r^\infty(t-\tau)] \begin{Bmatrix} \{0\} \\ u_b^t(\tau) \end{Bmatrix} d\tau \right\} \\ & = \left\{ \begin{Bmatrix} \{0\} \\ [C_\infty] \{ \dot{u}_b^g(t) \} + [K_\infty] \{ u_b^g(t) \} + \int_0^t [S_r^\infty(t-\tau)] \{ u_b^t(\tau) \} d\tau \end{Bmatrix} \right\} \quad (9) \end{aligned}$$

UCSD soil model

The UCSD soil model has been implemented for the finite elements of the free-field pressure dependent sandy soil. Fig.3 illustrates shear stress – strain behaviour of this multi-yield surface constitutive model.

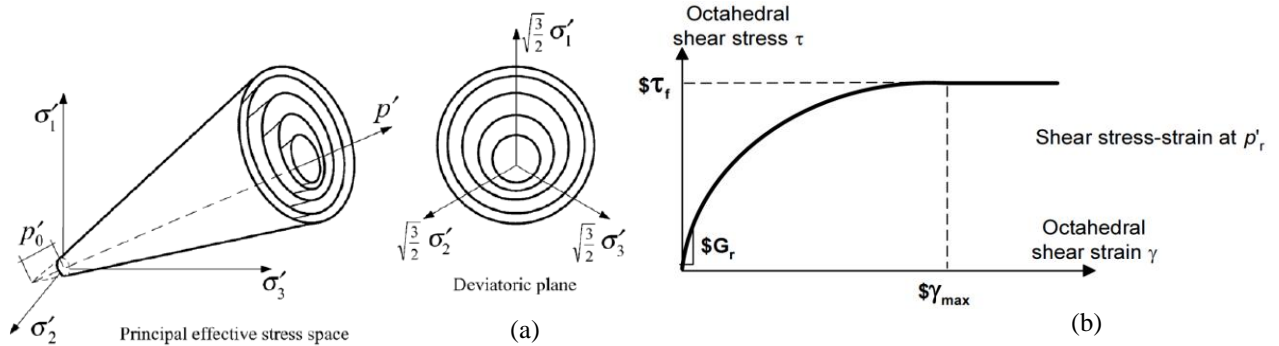


Figure 3. (a) UCSD soil model in principal effective stress space and deviatoric plane, (b) Octahedral shear stress vs. shear strain (after Zh. Yang et al., 2008)

where p'_r is the reference mean effective confining pressure at which G_r , B_r and γ_{max} are defined. G_r , B_r and γ_{max} are respectively reference low-strain shear modulus, reference bulk modulus and the maximum shear strength at which the maximum shear strength is reached. σ'_1 , σ'_2 and σ'_3 are effective principal stresses. γ is defined in Eq.(10):

$$\gamma = 2 / 3 \left[(\xi_{xx} - \xi_{yy})^2 + (\xi_{yy} - \xi_{zz})^2 + (\xi_{xx} - \xi_{zz})^2 + y\xi_{xy}^2 + y\xi_{yz}^2 + y\xi_{xz}^2 \right]^{1/2} \quad (10)$$

τ_f is the maximum octahedral shear strength which is related to the effective confining pressure by the internal friction angle of the soil as shown in Eq.(11):

$$\tau_f = \frac{2\sqrt{2} \sin \varphi}{3 - \sin \varphi} p' \quad (11)$$

And the total octahedral stress equation will be as Eq.(12):

$$\tau = 1 / 3 \left[(\sigma_{xx} - \sigma_{yy})^2 + (\sigma_{yy} - \sigma_{zz})^2 + (\sigma_{xx} - \sigma_{zz})^2 + y\sigma_{xy}^2 + y\sigma_{yz}^2 + y\sigma_{xz}^2 \right]^{1/2} \quad (12)$$

A hyperbolic relation holds for the backbone curve of nonlinear stress-strain diagram in constant confining pressure, as in Eq.(13):

$$\tau = \frac{G\gamma}{1 + \frac{\gamma}{\gamma_r} \left(\frac{p_r}{p'} \right)^d} \quad (13)$$

d being a curve fitting constant which is also used to define variations of G and B as a function of instantaneous effective confinement p' , also named '*Pressure Dependence Coefficient*':

$$G = G_r \left(\frac{p'}{p_r} \right)^d \quad (14.a)$$

$$B = B_r \left(\frac{p'}{p_r} \right)^d \quad (14.b)$$

To keep the constitutive model calibrated, the equations of γ_r (subscript r stands for '*reference*' in all denotations) must satisfy Eq.(15) in p' :

$\tau_f = \frac{2\sqrt{2}\sin\varphi}{3 - \sin\varphi} p_r = \frac{G_r \gamma_{MAX}}{1 + \gamma_{MAX} / \gamma_r} \quad (15)$	
---	--

Finally, Eq.(16) defines the internal friction angle of the sandy soil:

$$\sin\varphi = \frac{3\sqrt{3}\sigma_m / p_r}{6 + \sqrt{3}\sigma_m / p_r} \quad (16)$$

σ_m being the product of the last modulus and strain pair in the modulus reduction curve (Yang et al., 2008).

MODEL DESCRIPTION

Physical model

A 6-story reinforced concrete frame whose foundation upper surface is 2 meters below the surface of the soil is modelled on the near-field sandy soil. Fig.4 depicts a scheme of the problem.

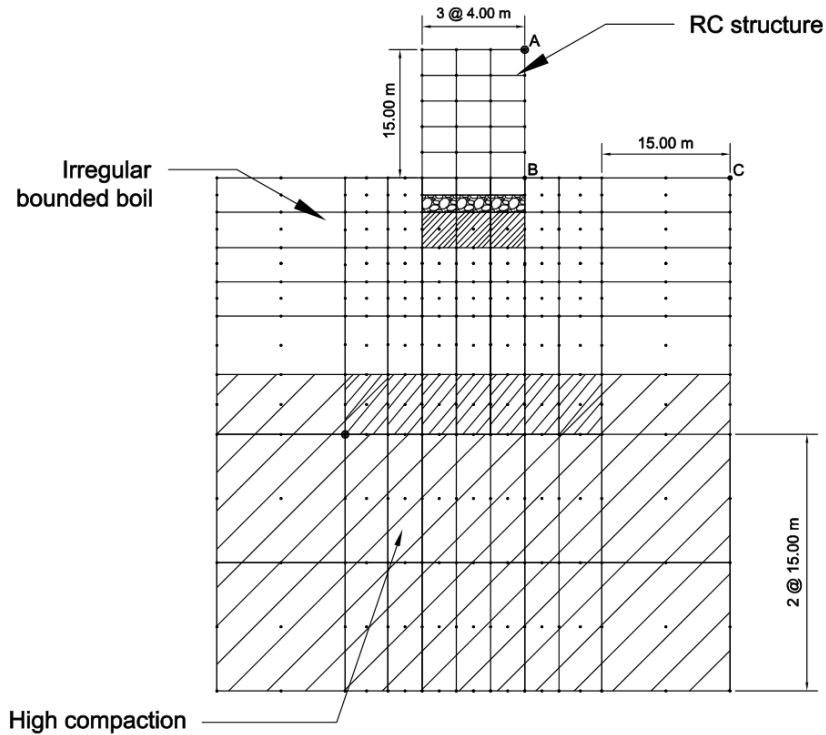
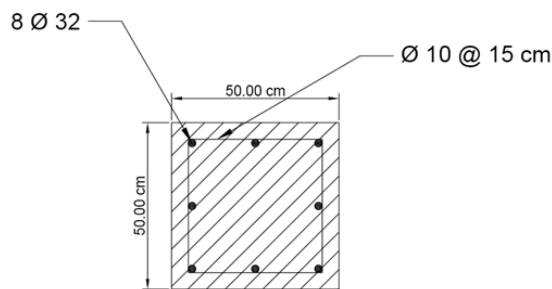


Figure 4. Near-field soil along with the RC frame placed upon

The cross section of beam and column elements of the structure, which may behave nonlinearly when exposed to (seismic) loads, is shown in Fig.5. The axial and flexural stiffnesses denoted below Fig.5 correspond to the case in which the structure responds linearly elastic.



Columns & Beams Section

$$EA = 1.91e7 \text{ kN}$$

$$EI = 156420 \text{ kNm}^2$$

Figure 5. Beam and column elements cross section

Table.1, Table.2 and Table.3 present the mechanical properties used to define soil and structure materials.

Table 1. Mechanical properties of concrete for nonlinear structure

Mechanical Properties	Characteristic Strength (kPa)	Strain in Maximum Strength	Crushing Strength (kPa)	Strain before Crushing	Tension Strength (kPa)
Core Concrete	24×10^{-3}	0.0024	5.6×10^{-3}	0.015	0
Cover Concrete	21×10^{-3}	0.002	5×10^{-3}	0.005	0

Table 2. Mechanical properties of steel for nonlinear structure

Mechanical Properties	Yield Stress (kPa)	Initial Modulus of Elasticity (kPa)	Strain Hardening Ratio
Reinforcing Steel	420×10^3	2×10^8	0.01

Table 3. Mechanical properties of near-field nonlinear sandy soil

Soil Properties	Mass Density (ton/m ³)	Reference Shear Modulus (kPa)	Reference Bulk Modulus (kPa)	Friction Angle	Phase Transformation Angle	Peak Shear Strain	Reference Pressure (kPa)	Pressure Dependence Coefficient (d)	Porosity
D < 23 m	1.9	7.5×10^4	2.0×10^5	33	27	0.1	80	0.5	0.7
D > 23 m	2.1	1.3×10^5	3.9×10^5	40	27	0.1	80	0.5	0.45

Table.4 represents the geometric properties of the RC frames whose structural responses are of favour for the results of this study.

Table 4. Geometric properties of the RC frame

Number of Stories	Typical Story Height (m)	Basement Story Height (m)	Number of Intervals	Length of Intervals (m)	Foundation Type	Load per Unit Length of Beam Elements (kNm ⁻¹)
6	3	2	3	4	Rigid	50

As mentioned earlier, soil elements are modelled based on UCSD soil constitutive model. Each element of soil consists of nine nodes, each three placed on one side at equal distances the ninth of which rests in the centre of the quadrilateral element. Fig.6 presents a typical quadrilateral element and its node numbering order.

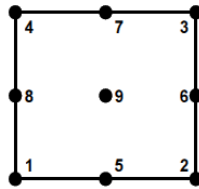


Figure 6. Typical quadrilateral soil element (after Zh. Yang et al., 2008)

Motions

Horizontal and vertical free-field motions of Loma Prieta earthquake (1989) records shown respectively in Fig.6 and Fig.7 were considered for the analyses.

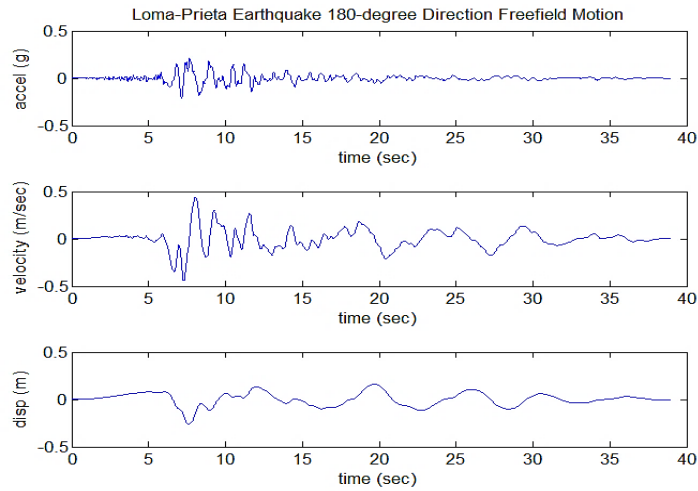


Figure 6. Acceleration, velocity and displacement time histories of free-field NS component of Loma Prieta recorded during 1989 earthquake, scaled to g

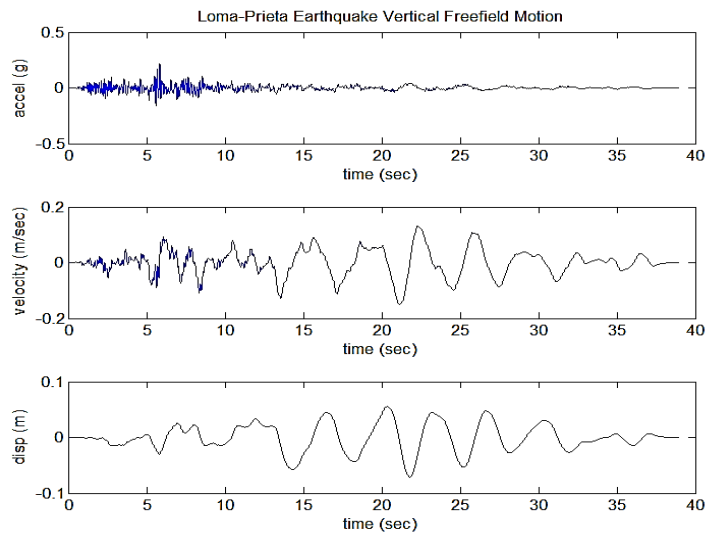


Figure 7. Acceleration, velocity and displacement time histories of free-field vertical component of Loma Prieta recorded during 1989 earthquake, scaled to g

The ground system including the interface on which interaction forces are calculated is illustrated in Fig.8. The depth with recognizable plastic behaviour, i.e. depth and length of hypothetical excavation D , has been supposed to be equal to 60 meters in this study.

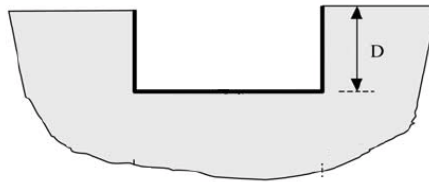


Figure 8. Ground with excavation constituting interface nodes on fictitious boundary

EFFECTIVE INPUT MOTIONS

Using the Fourier transform, the Fourier amplitude spectrum has been obtained and applying the dynamic stiffness multiplier gained from SBFEM, the Fourier amplitude spectrum of the effective

input motion to the interface yields. At last, through an inverse Fourier Transform, the resulting motion follows. Results are presented primarily for acceleration time histories. Fig.9 and Fig.10 present the procedure for horizontal and vertical motions respectively.

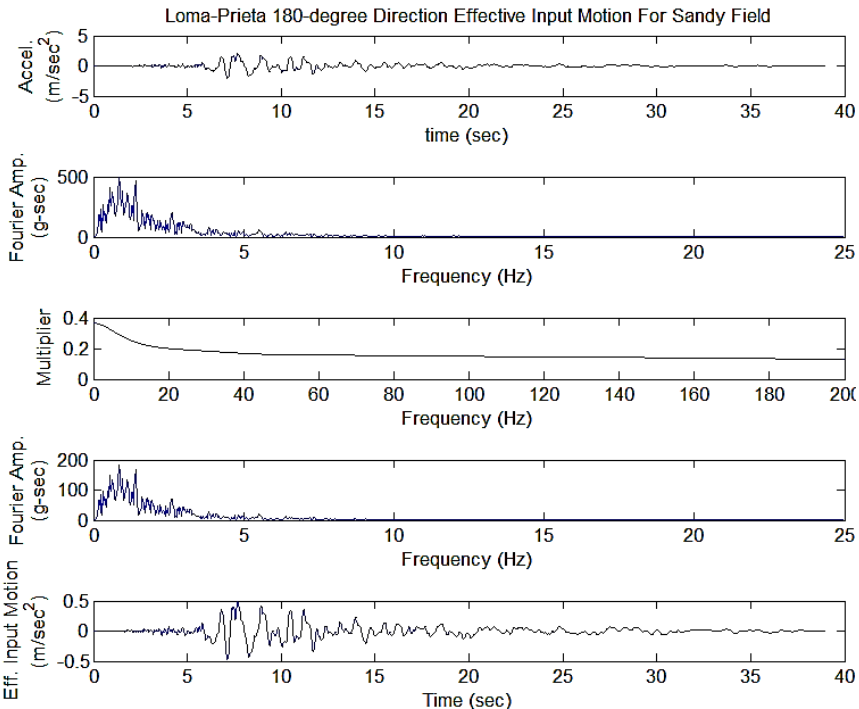


Figure 9. Loma Prieta horizontal effective input motion for sandy field

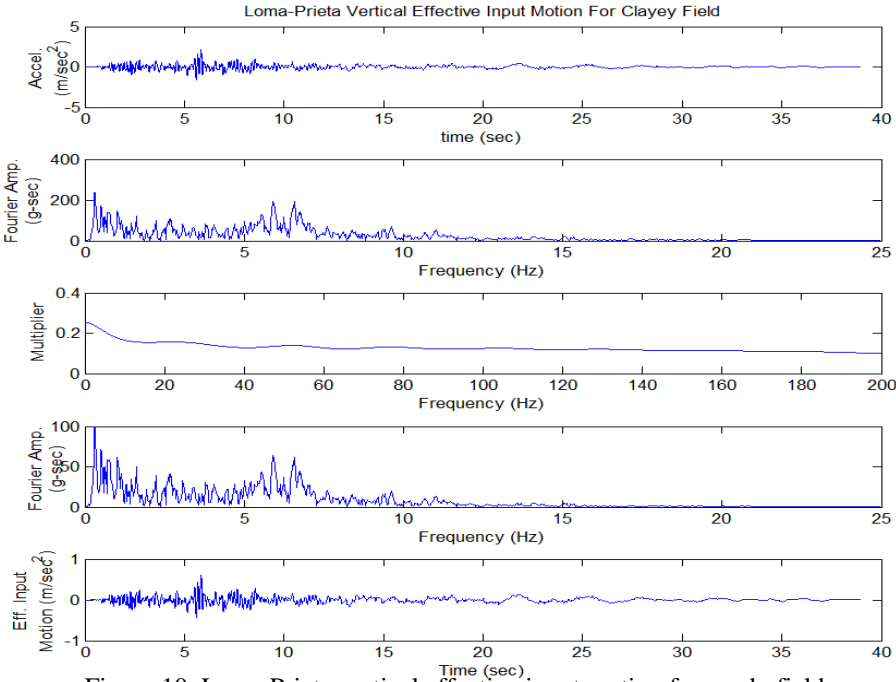


Figure 10. Loma Prieta vertical effective input motion for sandy field

The multiplier seems to be more influential on the strong motion component of the frequency content of the motion. It reduces higher frequencies much more than lower frequencies which are of greater amplitudes. So, although not totally filtered out, the high frequency component of the motion is subject to more reduction altering from free-field to ground.

INTERACTION FORCES

After determining the effective input motions to the interface of the media, the path will be open to carry out the calculation of interaction forces using convolution integrals. The most important factor to determine these forces is the unit impulse response. The virtual impulse time in which the peak of the impulse falls is supposed 1 second. The progression with discretized time is presented in Fig.11 for incompressible and compressible conditions of the soil that will later correspond to undrained and drained near-field conditions respectively.

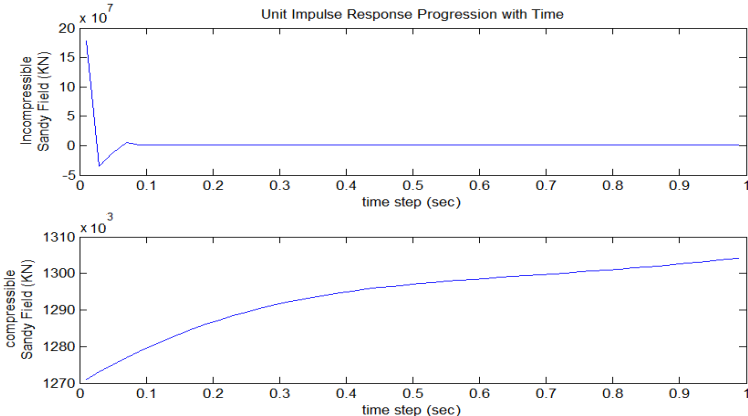


Figure 11. Unit impulse response of the ground obtained from SBFEM for incompressible and compressible sandy fields

Fig.11 reveals the difference between response origins of sites with and without drainage contrivances. It is observed that to a unit impulse, the incompressible site reveals its maximum reaction instantaneously unlike for the incompressible condition. Fig.12 illustrates the interaction forces to the generalized structure-unbounded soil interface for the two mentioned materials. The generalized structure refers to the structure plus the near-field soil, both of which may act nonlinearly when exposed to cyclic or monotonic loads of any kind.

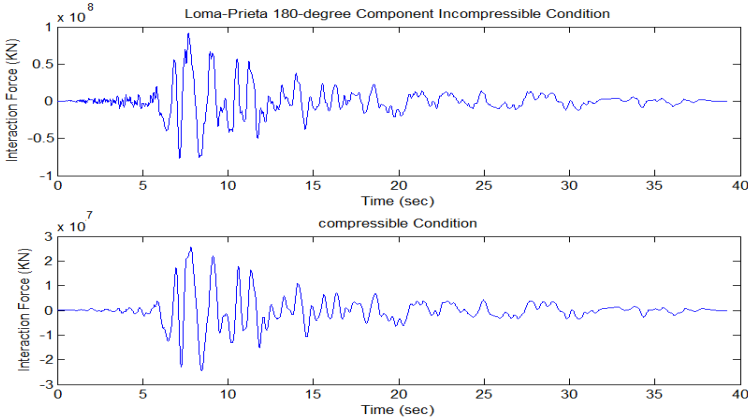


Figure 12. Horizontal interaction forces for incompressible and compressible sandy soil

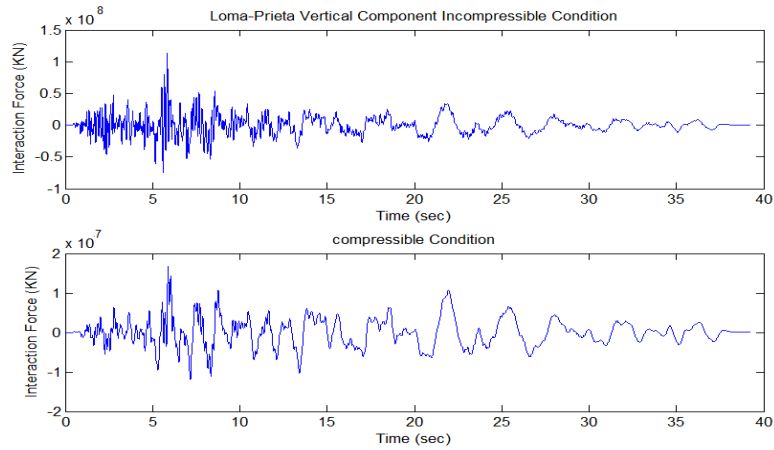


Figure 13. Vertical interaction forces for incompressible and compressible sandy soil

It can be inferred from the figures that the greater interaction force relates to the incompressible condition, which corresponds to liquefaction assumptions and experiments. On the other hand, the forces are smoother for the compressible case and the frequency content is much milder. The force time-histories show a very short time delay with the free-field motion which is sensible from a practical point of view.

STRUCTURAL RESPONSES

Displacements

Responses of the structure with fixed base as well as when subject to elastic and elastoplastic seismic soil-structure interaction have been recorded and are of interest. The case of conventional elastic-plastic soil behaviour developed by scientists such as Terzaghi and Meyerhof has been included too. Fig.14 illustrates a comparison between structural response amplitudes in its height for different states of sandy soil under the structure.

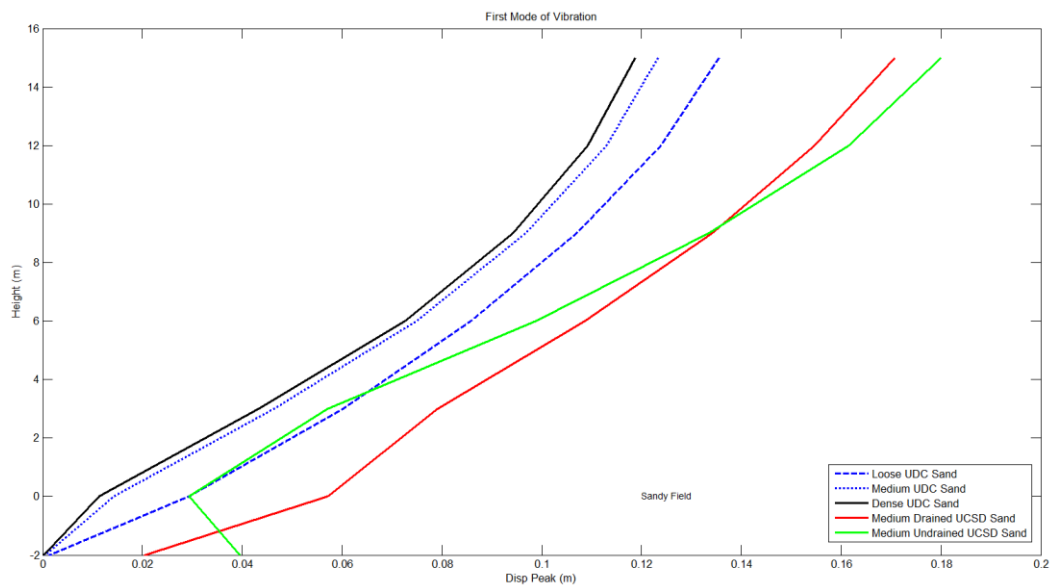


Figure 14. Structural displacement amplitudes in its height for different sand states under the foundation

As is observed from the graphs, the denser the soil gets the less the displacements will be; and this means the role of the underlying soil in seismic displacements lessens which is logical and obvious. Drainage of the soil results in bigger displacements for heights less than 9 meters and smaller displacements for the higher compared to the undrained case. When the soil is undrained, the movement of the stories above the ground will not necessarily be more than those below the surface including the basemat. No discrepancies are observed in displacement amplitudes from one state to another of the soil for conventional behaviour assumptions, while, for the UCSD model which implements drainage of the soil, these discrepancies are observed.

Base shears

The state and properties of the underlying soil not only affects the displacements of the structure above, but will also result in different force distribution patterns from the ground to the structure. Fig.15 depicts variations of base shear time history with changes in soil conditions.

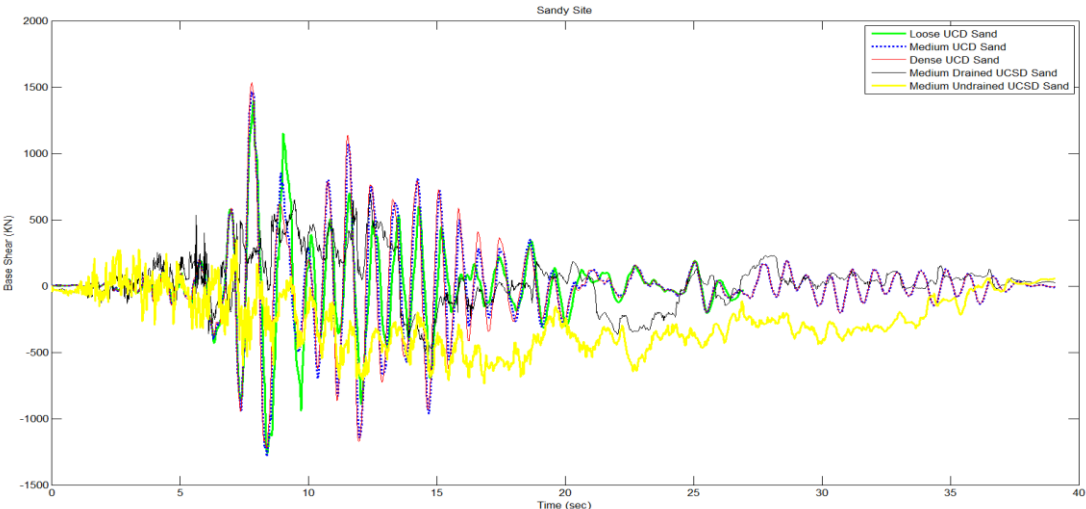


Figure 15. Time history of base shears for different conditions of sand

The figure above states that the base shear time history trend for the undrained soil is different from that of other cases. Based on this figure, although for the UCSD model the maximum base shear is less than that of other cases, it lasts longer and its mean varies slowly after it meets the maximum until the motion ends. The sustenance of this long lasting relatively high base shear may even cause severer damages to the structure especially for longer lasting quakes although the peak is not as high. As is clear from the figure, the denser the soil gets the more the base shears will be.

CONCLUSIONS

An RC frame was modelled on potentially elastoplastic sandy soil the far-field of which was modelled with the SBFEM method substituted by interaction forces through convolution integrals using the unit impulse response of the medium. For the drained case, the interaction forces are much less than that for the undrained case and the interaction forces time history is smoother. The near-field soil was modelled by finite elements implemented by the UCSD soil model and responses of the structure were captured in the sense of forces and displacement amplitudes. It was observed that considering drainage potential for the sand results in discrepancies of displacement amplitudes in the height of the structure. In case the soil is undrained, the displacements of the basemat of the structure may be more than those of the bottom stories at times. Also, drainage potential affects the base shear such that the soil in which the state of being drained/undrained can be modelled reveals smaller but more extended-in-time base

shear maxima. Results suggest that the denser the soil gets, the smaller the interaction-induced displacements yet the bigger support reactions and base shears will be.

ACKNOWLEDGEMENTS

Hereby the authors wish to thank professor M.C. Genes from Zirve University, Gaziantep, Turkey for his very valuable comments on analysis procedures using SBFEM and for precious references offered. Dr. A. Lashkari from Shiraz University of Technology is to be acknowledged for his precious comments on soil constitutive modelling. This study was carried out under the support of Shiraz University of Technology for the proceedings of the 2nd European Conference on Earthquake Engineering and Seismology. Reviewers are to be thanked gratefully for their insight into the matter and their kind remarks.

REFERENCES

- Genes, M. & Kocak, S. 2002. Seismic Analyses of Soil Structure Interaction Systems by Coupling the Finite Element and the Scaled Boundary Finite Element Methods
- Genes, M. C. 2012. Dynamic analysis of large-scale SSI systems for layered unbounded media via a parallelized coupled finite-element/boundary-element/scaled boundary finite-element model. *Engineering Analysis with Boundary Elements*, 36, 845-857
- Genes, M. C. & Kocak, S. 2005. Dynamic soil–structure interaction analysis of layered unbounded media via a coupled finite element/boundary element/scaled boundary finite element model. *International Journal for Numerical Methods in Engineering*, 62, 798-823
- Hassanen, M. & El-Hamalawi, A. 2007. Two-dimensional development of the dynamic coupled consolidation scaled boundary finite-element method for fully saturated soils. *Soil Dynamics and Earthquake Engineering*, 27, 153-165
- Kramer, S. 1996. Geotechnical earthquake engineering. 1996. *Practice Hall, New Jersey, 653pp*
- Kutanis, M. & Elmas, M. 2009. Non-Linear Seismic Soil-Structure Interaction Analysis Based on the Substructure Method in the Time Domain. *Turkish Journal of Engineering and Environmental Sciences*, 25, 617-626
- Mohasseb, S. K. & Wolf, J. P. 1989. Recursive evaluation of interaction forces of unbounded soil in frequency domain. *Soil Dynamics and Earthquake Engineering*, 8, 176-188
- Noorzaei, J., Viladkar, M. & Godbole, P. 1995. Elasto-plastic analysis for soil-structure interaction in framed structures. *Computers & structures*, 55, 797-807
- Wolf, J. P. 1985. *Dynamic soil-structure interaction*, Prentice Hall int
- Wolf, J. P. 2003. The scaled boundary finite element method, John Wiley & Sons Inc
- Wolf, J. P. & Song, C. 1996. *Finite-element modelling of unbounded media*, Wiley Chichester
- Yang, Z., Lu, J. & Elgamal, A. 2008. OpenSees soil models and solid-fluid fully coupled elements: user's manual, Version 1. *San Diego: University of California*